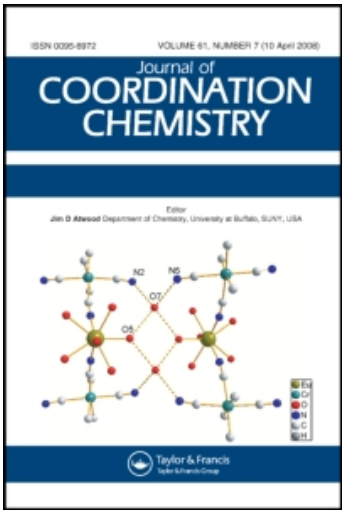

Journal of Coordination Chemistry
Publication details, including instructions for authors and subscription information:
http://www.informaworld.com/smpp/title~content=t713455674

Electrochemical studies of the *bis* (triphenyl phosphine) ruthenium(II) complex, *cis* -[$RuCl_2(L)(PPh_3)_2$], with L = 2-(2'-pyridyl)quinoxaline

Nikos G. Tsierkezos[a]; Uwe Ritter[a]; Athanassios I. Philippopoulos[b]; Detlef Schröder[c]
[a] Institut für Chemie, Elektrochemie und Galvanotechnik, Fachgebiet Chemie, Technische Universität Ilmenau, Weimarer Straße 25, 98693 Ilmenau, Germany [b] Laboratory of Inorganic Chemistry, Faculty of Chemistry, School of Science, National and Kapodistrian University of Athens, Panepistimiopolis Zografou 15771, Athens, Greece [c] Institute of Organic Chemistry and Biochemistry, Academy of Sciences of the Czech Republic, Flemingovo náměsti 2, 166 10 Prague 6, Czech Republic

First published on: 14 September 2010

To cite this Article Tsierkezos, Nikos G. , Ritter, Uwe , Philippopoulos, Athanassios I. and Schröder, Detlef(2010) 'Electrochemical studies of the *bis* (triphenyl phosphine) ruthenium(II) complex, *cis* -[$RuCl_2(L)(PPh_3)_2$], with L = 2-(2'-pyridyl)quinoxaline', Journal of Coordination Chemistry, 63: 20, 3517 — 3530, First published on: 14 September 2010 (iFirst)
To link to this Article: DOI: 10.1080/00958972.2010.516362
URL: http://dx.doi.org/10.1080/00958972.2010.516362

Journal of Coordination Chemistry
Vol. 63, No. 20, 20 October 2010, 3517–3530

Electrochemical studies of the *bis*(triphenyl phosphine) ruthenium(II) complex, *cis*-[$RuCl_2(L)(PPh_3)_2$], with L = 2-(2′-pyridyl)quinoxaline

NIKOS G. TSIERKEZOS*†, UWE RITTER†, ATHANASSIOS I. PHILIPPOPOULOS‡ and DETLEF SCHRÖDER§

†Institut für Chemie, Elektrochemie und Galvanotechnik, Fachgebiet Chemie, Technische Universität Ilmenau, Weimarer Straße 25, 98693 Ilmenau, Germany
‡Laboratory of Inorganic Chemistry, Faculty of Chemistry, School of Science, National and Kapodistrian University of Athens, Panepistimiopolis Zografou 15771, Athens, Greece
§Institute of Organic Chemistry and Biochemistry, Academy of Sciences of the Czech Republic, Flemingovo náměsti 2, 166 10 Prague 6, Czech Republic

(*Received 7 May 2010; in final form 21 July 2010*)

Electrochemical studies of the newly synthesized *bis*(triphenyl phosphine) ruthenium(II) complex, *cis*-[$RuCl_2(L)(PPh_3)_2$] (**1**, with L = 2-(2′-pyridyl)quinoxaline, $C_{13}N_3H_9$), were performed in acetonitrile (ACN). For this purpose, cyclic voltammograms (CVs) as well as electrochemical impedance spectra (EIS) were recorded on either glassy carbon (GC), platinum (Pt), gold (Au), or multi-walled carbon nanotube (MWCNT) electrodes. Qualitative examination of solutions of **1** in ACN was performed on the basis of conductivity measurements and electrospray ionization mass spectrometry (ESI–MS). The conductivity data suggest that **1** is a 1 : 1 type electrolyte in ACN. The ESI spectra further demonstrate that upon dissolution of **1** in ACN progressive replacement of chloro- and PPh_3-ligands by ACN occurs, leading to formation of $[RuCl(L)(PPh_3)(CH_3CN)_2]^+Cl^-$, [$\mathbf{2^+Cl^-}$]. The CVs recorded for [$\mathbf{2^+Cl^-}$] on various working electrodes demonstrate that the reversibility of the redox couple $\mathbf{2^{2+/+}}$ enhances with the order: Au < Pt < MWCNT < GC. The EI spectra verify that GC and MWCNT electrodes provide insignificant barrier for interfacial electron transfer since they afford less charge-transfer resistance.

Keywords: Conductivity; Cyclic voltammetry; Electrochemical impedance spectrometry; Electrospray ionization mass spectrometry; Ruthenium(II) complex

1. Introduction

Coordination chemistry of ruthenium receives considerable interest from a large number of scientists with spectroscopic and electrochemical studies on either mononuclear or binuclear ruthenium complexes with a large variety of ligands performed [1–10]. In these studies, however, most attention was focused on

*Corresponding author. Email: nikos.tsierkezos@tu-ilmenau.de

ISSN 0095-8972 print/ISSN 1029-0389 online © 2010 Taylor & Francis
DOI: 10.1080/00958972.2010.516362

pyridine-type complexes, which are chemically stable and exhibit interesting redox properties as well as photophysical characteristics. Consequently, a large variety of such complexes were synthesized and used as photosensitizers in several intermolecular photochemical processes [11–16]. Also, fullerene polypyridine ligands were synthesized and their coordination to ruthenium(II) was investigated [17]. Furthermore, some ferrocenoyl-pyridine arene ruthenium complexes were recently synthesized and extensively studied due to their anticancer properties [18]. In addition to the pyridine-type complexes, ruthenium complexes having phosphine ligands have also attracted significant interest, since they are efficient catalysts in homogeneous catalyzed hydrogenation reactions [19–21]. For example, one of the most important mechanisms for hydrogenation of imines and ketones, which was recently proposed, involved mixed ruthenium phosphine and diamine complexes [22]. In addition, ruthenium complexes with anionic phosphine ligands were found to be efficient in the catalytic cyclopropanation reaction of olefins with ethyl diazoacetate [23]. Furthermore, some aqua ruthenium(II) complexes containing phosphine- and polypyridine-ligands were used for electrocatalytic oxidation of various alcohols [24]. Considering the importance of the phosphine-type complexes of ruthenium, we report, in this article, an extensive electrochemical study, in acetonitrile (ACN), on the newly synthesized Ru(II) complex *bis*(triphenyl phosphine) ruthenium(II), *cis*-$[RuCl_2(L)(PPh_3)_2]$ (**1**), where L stands for the chelate ligand 2-(2′-pyridyl)quinoxaline ($C_{13}N_3H_9$) (Supplementary material, figure S1). Conductivity, cyclic voltammetry (CV), electrochemical impedance spectrometry (EIS), and electrospray ionization mass spectrometry (ESI–MS) were used. In the electrochemical experiments, four different working electrodes were tested, glassy carbon (GC), platinum (Pt), gold (Au), and a film consisting of multi-walled carbon nanotubes (MWCNTs) grown on oxidized silicon wafer (SiO_2/Si), recently prepared and characterized in our laboratory.

2. Experimental

2.1. *Materials*

2.1.1. Solvents and reagents. ACN (Merck, puriss grade), was pre-dried over anhydrous potassium carbonate and distilled over phosphorus pentoxide. The dried ACN was stored over 0.4 nm molecular sieve under argon and degassed under vacuum prior to all measurements. The electrolyte, *n*-tetrabutylammonium hexafluorophosphate, NBu_4PF_6 (Fluka, purum grade), was recrystallized twice from absolute ethanol and dried under reduced pressure at room temperature [25], while potassium chloride, KCl (Merck, puriss grade), was dried at 100°C.

2.1.2. Synthesis of *cis*-$[RuCl_2(L)(PPh_3)_2]$. The synthesis of *cis*-$[RuCl_2(L)(PPh_3)_2]$ (**1**) was carried out under argon using standard Schlenk techniques. The schematic presentation of the reaction for the synthesis of **1** is shown in figure S2 (Supplementary material). The starting materials, 2-(2′-pyridyl)quinoxaline (L) and $[RuCl_2(PPh_3)_3]$, were prepared according to procedures reported in the literature [26, 27]. Experimental

details for the synthesis of **1**, as well as spectroscopic data, were reported in a previous paper [28].

2.2. *Solutions*

For conductivity measurements, a stock solution of **1** (1.5×10^{-4} mol L^{-1}) in ACN was prepared, from which 10 different solutions in the concentration range from 3.0×10^{-5} to 1.3×10^{-4} mol L^{-1} were obtained by dilution. For the CV and EIS experiments, the supporting electrolyte NBu_4PF_6 (0.10 mol L^{-1}) was used in conjunction with dilute solutions of **1** (1.0×10^{-4} mol L^{-1}) in ACN. Likewise, the ESI–MS experiments were performed with 1.5×10^{-4} mol L^{-1} solution of **1** in ACN. In all cases, the solutions were prepared by mass with an uncertainty of ±0.0001 g (Sartorius, AG 204). The conversion of molonity (m, mol kg^{-1}) to molarity (c, mol L^{-1}) was done using the density values of the solvent. All solutions were prepared under argon using Schlenk techniques.

2.3. *Apparatus and procedures*

2.3.1. Conductivity. The conductance measurements were carried out with a digital bridge-type conductivity meter (Metrohm 712). A conductance cell (dipping type) with platinum black electrode was used. The cell constant (0.81 cm^{-1}) was determined by measuring aqueous solutions of KCl in the concentration range from 1.0×10^{-3} to 0.10 mol L^{-1} [29]. The electrode was cleaned first with a nitric acid solution and then with distilled water, and finally dried with acetone. The cell was thermostated at 21.0°C using a water bath, while its temperature was controlled with a digital thermometer. All conductivity data were corrected with the specific conductivity of ACN, as detailed elsewhere [30, 31].

2.3.2. Cyclic voltammetry. Cyclic voltammograms (CVs) were recorded using a computer-controlled system Zahner/IM6/6EX and analyzed using the Thales software (version 4.15). The effect of uncompensated resistance was reduced by using the positive feedback technique. For this purpose, each CV was recorded several times using an experimental setup, in which the uncompensated resistance was gradually compensated. The measurements were carried out using a three-electrode cell configuration. The working electrodes used were either GC wire (9 mm length), Pt wire (7 mm length), Au disk (2.8 mm diameter), or MWCNT film (geometrical area 0.5 cm^2); the counter electrode was a Pt plate (1.0 cm^2). All potentials were recorded relative to Ag/AgCl (KCl sat.) reference electrode. The MWCNT film was synthesized on SiO_2/Si substrate in a furnace at 900°C by catalytic chemical vapor deposition (CVD) using ferrocene (1% w/w) as catalyst and benzene as carbon source [32–34]. Representative scanning electron microscopy (SEM) and transmission electron microscopy (TEM) images of the synthesized MWCNT film are shown in figure S3 (Supplementary material). A three-compartment electrochemical cell designed to minimize the distances between the electrodes with a total solution volume of ~20 mL was used. The CVs were recorded in the potential region from −1.5 to 0 V *versus* Ag/AgCl with scan rates (v) ranging from 0.02 to 0.12 V s^{-1}. All measurements were carried out at room temperature, 21.0°C.

2.3.3. Electrochemical impedance spectroscopy. Electrochemical impedance spectra (EIS) were recorded using the computer-controlled system Zahner/IM6/6EX by applying small ac amplitude (10 mV) in a wide frequency range (from 0.1 Hz to 50 kHz) at 21.0°C. All measurements were performed on either GC, Pt, Au, or MWCNT working electrodes against the reference electrode Ag/AgCl (KCl sat.), while a Pt plate served as counter electrode. In all cases the EIS were recorded in a potential which corresponds to the half-wave potential ($E_{1/2}$) of the investigated $\mathbf{2}^{2+/+}$ redox couple. The EIS were analyzed using the Thales software (version 4.15). For analysis of the recorded EIS, the electrical circuits shown in figures S8 and S9 were applied.

2.3.4. Electrospray ionization mass spectrometry. ESI–MS experiments were performed with a TSQ Classic mass spectrometer, which consists of an ESI source followed by a tandem mass spectrometer of QOQ configuration (where Q stands for quadrupole and O for octopole) [35, 36]. In the experiments, a solution of **1** in ACN was introduced *via* a syringe pump (flow rate of 5 μL min^{-1}) to the fused-silica capillary of the ESI source. The temperature of the heated capillary was maintained at 200°C. Nitrogen was used as nebulizing gas. Mass spectra of the ions formed were obtained at unit mass resolution by scanning the first quadrupole. The size of the solvated gaseous ions generated in ESI depends on the source conditions, which can be varied from very soft to quite hard [37, 38]. It has to be mentioned, however, that soft conditions were applied in this study. For collision-induced dissociation (CID) experiments, the gaseous ions of interest were mass-selected in the first quadrupole, interacted with xenon at pressures between $0.5–3.0 \times 10^{-4}$ mbar in the octopole collision chamber at various collision energies ($E_{Lab} = 0–24$ eV), while the resulting ionic fragments were detected by means of the second quadrupole.

3. Results and discussion

3.1. *Conductance data and ESI–MS*

The measured specific conductivity (k) values of solutions of **1** in ACN, in the concentration range from 3.0×10^{-5} to 1.3×10^{-4} mol L^{-1}, are rather large and show a linear dependence on solute concentration (Supplementary material, figure S4). Hence, it can be concluded that dissolved **1** behaves as a strong electrolyte in ACN. The determined molar conductivities (Λ) in ACN were in the range $\Lambda = 120–160$ S cm^2 mol^{-1}, which is within the range suggested for simple 1 : 1 electrolytes [39–42] and their complex ions in ACN [43, 44]. This conductivity can be explained by replacement of a chloro ligand by solvent, which leads to the formation of the 1 : 1 electrolyte $[RuCl(L)(PPh_3)_2(CH_3CN)]^+Cl^-$. According to the experimental conductivity values, the second chloro ligand does not undergo exchange by another ACN molecule, because this would lead to a 2 : 1 type electrolyte for which the resulting Λ would be much larger (the suggested range for 2 : 1 electrolytes in ACN is $\Lambda = 220–300$ S cm^2 mol^{-1}) [44].

Unfortunately, the conductivity data do not provide further information for possible replacement of the neutral ligands, such as L and PPh_3, since such substitutions would not modify the type of the electrolyte, and thus would have no influence on net

conductivity of the solution. In order to obtain qualitative information regarding the type of species present, a solution of **1** in ACN was analyzed by ESI–MS. The ESI–MS method was chosen because the ions formed upon ESI under soft ionization conditions correlate with the species that exist in solution [45–48]. Representative ESI–MS spectra recorded for **1** in ACN under soft ionization conditions at different time periods are shown in figure 1. The main peaks observed in the ESI spectra correspond, according to

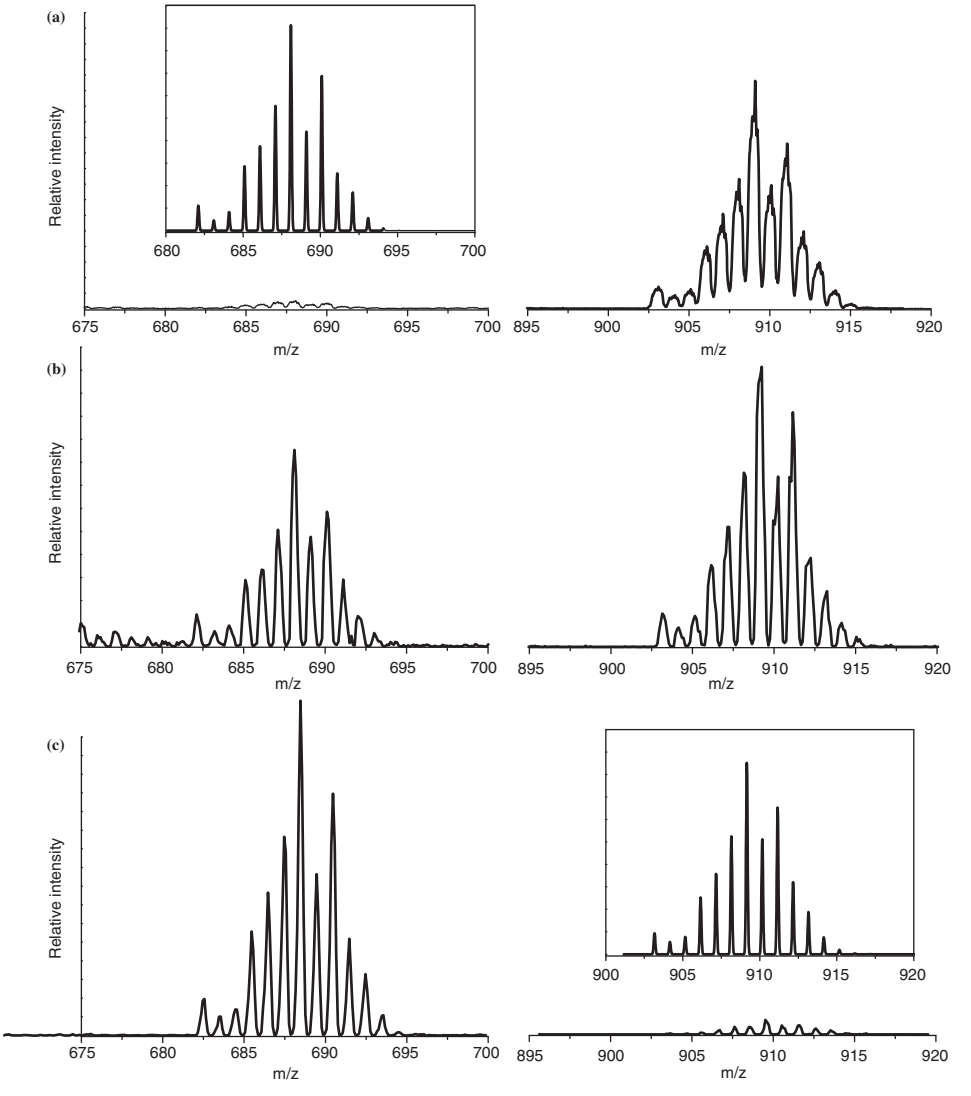

Figure 1. ESI–MS spectra recorded for 1 in ACN under soft ionization conditions in various time periods. The ESI–MS spectra are denoted as follows: (a) ESI–MS spectrum recorded initially, (b) after 7 h, and (c) after 24 h. The observed signals at m/z 688 and m/z 909 correspond to the gaseous ions $[RuCl(L)(PPh_3)(CH_3CN)_2]^+$ and $[RuCl(L)(PPh_3)_2(CH_3CN)]^+$, respectively. The ESI–MS spectra indicate the progressive formation of $[RuCl(L)(PPh_3)(CH_3CN)_2]^+$ and breakdown of $[RuCl(L)(PPh_3)_2(CH_3CN)]^+$. The insets exhibit their simulated isotope profiles.

their ion masses and their isotope patterns, to the ruthenium(II) gaseous monocations $[RuCl(L)(PPh_3)(CH_3CN)_2]^+$ (m/z 688) and $[RuCl(L)(PPh_3)_2(CH_3CN)]^+$ (m/z 908). Surprisingly, the intensities of the observed peaks in the ESI spectrum vary significantly with time. Namely, the ESI spectrum recorded immediately after the preparation of the solution yields $[RuCl(L)(PPh_3)_2(CH_3CN)]^+$ as the dominant species, while the ESI spectrum obtained several hours later is dominated by $[RuCl(L)(PPh_3)(CH_3CN)_2]^+$. These findings are fully consistent with the above conclusion that during the dissolution of **1** in ACN, one chloride is replaced by ACN (reaction 1). However, along with the replacement of the chloride, a slow exchange of one of the PPh_3-ligands is observed (reaction 2). Notably, no further exchange of the second chlorine or PPh_3 by ACN is observed.

$$[RuCl_2(L)(PPh_3)_2] + CH_3CN \rightarrow [RuCl(L)(PPh_3)_2(CH_3CN)]^+ + Cl^- \quad (1)$$

$$[RuCl(L)(PPh_3)_2(CH_3CN)]^+ + CH_3CN \rightarrow [RuCl(L)(PPh_3)_2(CH_3CN_2)]^+ + PPh_3 \quad (2)$$

The CID spectra of either $[RuCl(L)(PPh_3)_2(CH_3CN)]^+$ or $[RuCl(L)(PPh_3)(CH_3CN)_2]^+$, recorded in the collision-energy range 0–24 eV, reveal eliminations of neutral CH_3CN, PPh_3, and HCl as the main fragmentation processes. As an example, the CID breakdown diagram of $[RuCl(L)(PPh_3)_2(CH_3CN)]^+$ is shown in figure S5 (Supplementary material). The loss of CH_3CN already occurs at about $E_{Lab} = 4$ eV, whereas the onset of the loss of PPh_3 lies at about $E_{Lab} = 8$ eV. The HCl elimination takes place at enhanced collision energies (at about $E_{Lab} = 16$ eV).

The electrospray spectra imply that during the dissolution of **1** in ACN, one chloro- and one PPh_3 ligand are progressively replaced by ACN, and consequently the 1 : 1 type electrolyte $[RuCl(L)(PPh_3)(CH_3CN)_2]Cl$ (further referred as $[\mathbf{2^+Cl^-}]$), is formed. Similar behavior was observed in dimethyl sulfoxide (DMSO) solutions, namely, upon dissolution of **1** in DMSO formation of $[RuCl(L)(PPh_3)(DMSO)_2]Cl$ was observed [28]. Given that ACN supports the dissociation of electrolytes, since it is a polar medium with high dielectric constant ($\mu = 3.48$ D, $\varepsilon = 35.95$ at 25°C) [49], it is expected that $[\mathbf{2^+Cl^-}]$ dissociates into $\mathbf{2^+}$ and Cl^- ions and thereby significantly contributes to the total conductivity of the solution. Further analysis of the obtained conductivity data using the Lee–Wheaton model [50, 51] demonstrates that the limiting molar conductivity (Λ_o) of $[\mathbf{2^+Cl^-}]$ in ACN is $\Lambda_o = 165.3\ S\,cm^2\,mol^{-1}$, while its association constant (K_A) appears to be quite low ($K_A = 2.3\ mol^{-1}\,L$). The degree of dissociation (a_d) of $[\mathbf{2^+Cl^-}]$ in ACN in the investigated concentration range was determined to be nearly equal to unity ($0.9996 < a_d < 0.9999$), which indicates that $[\mathbf{2^+Cl^-}]$ can be considered as non-associated in ACN. Furthermore, the difference between the Λ_o value of $[\mathbf{2^+Cl^-}]$ in ACN ($\Lambda_o = 165.3\ S\,cm^2\,mol^{-1}$) reported in this study, and the Λ_o value measured in DMSO and reported in a previous article ($\Lambda_o = 29.8\ S\,cm^2\,mol^{-1}$, at 25°C) [28] can be attributed to the differences in the viscosity (η) of the solvent media ($\eta_{DMSO} = 1.948$ mPa s, $\eta_{ACN} = 0.361$ mPa s at 25°C) [52].

Displacement of Cl^- and PPh_3 by ACN was also observed by ^{31}P-NMR spectroscopy. The $^{31}P\{^1H\}$-NMR spectrum of **1** recorded in deuterated chloroform $CDCl_3$ reveals one single resonance at $\delta = 17.5$ ppm, which is characteristic for PPh_3-containing complexes in which the PPh_3 ligands are bound to metal in *trans* configuration. However, upon addition of dry ACN to **1** dissolved in $CDCl_3$, four new resonances appear in $^{31}P\{^1H\}$-NMR spectrum. One of these signals, at $\delta = -4.85$ ppm,

is attributed to "free" PPh_3 and the other three singlets at $\delta = 20.92$, 22.70, and 42.04 ppm correspond to phosphorus-containing species. The ratios of the integrated $^{31}P\{^1H\}$-NMR peaks at $\delta = -4.85$, 20.92, 22.70, and 42.04 ppm were 0.5/0.9/0.7/1.0, respectively.

3.2. *Cyclic voltammetry*

Representative CVs recorded for [$\mathbf{2^+Cl^-}$] in ACN on GC, Pt, Au, and MWCNT electrodes are shown in figure 2. In those CVs, [$\mathbf{2^+Cl^-}$] exhibits a single wave at all investigated electrodes, which seems to be either quasi-reversible or irreversible depending on the working electrode material. In detail, the well-shaped CVs recorded on GC (figure 2a) were found to be symmetric with equal cathodic (i_p^{red}) and anodic (i_p^{ox}) peak currents (thus, the ratio i_p^{ox}/i_p^{red} approaches unity) over the whole scan rate (v) range. Furthermore, variation of the anodic peak current (i_p^{ox}) with the square root of the scan rate was linear (inset figure 2a) with a slope proportional to the square root of the diffusion coefficient (D). From the slope of the plot (i_p^{ox}) *versus* $v^{1/2}$, the diffusion coefficient $D = 1.3 \times 10^{-5}\,cm^2\,s^{-1}$ was determined for the investigated electro-active compound in ACN. These findings indicate that concentrations of the oxidized and the reduced forms are equal and not consumed in a coupled chemical reaction, suggesting, therefore, that the charge-transfer process occurring on GC electrode is sufficiently fast to be classified as reversible or quasi-reversible. CVs recorded at different time periods are identical, indicating that the voltammetric responses of the initially dissolved **1** and its dissolution product [$\mathbf{2^+Cl^-}$] are similar. The oxidation peak, which corresponds to the one electron oxidation process, $\mathbf{2^+} \rightarrow \mathbf{2^{2+}} + e^-$, lies at the potential $E_p^{ox} = -0.733$ V *versus* Ag/AgCl (at $v = 0.02\,V\,s^{-1}$) and coexists with the reduction peak, corresponding to the inverse process (the reduction of $\mathbf{2^{2+}}$ to $\mathbf{2^+}$), and occurs at the potential $E_p^{red} = -0.903$ V *versus* Ag/AgCl (at $v = 0.02\,V\,s^{-1}$). Since the ligands used in this study are not reversibly reduced or oxidized within the potential limit +2.5 to −2.5 V (Supplementary material, figure S6), we believe that the redox process observed for [$\mathbf{2^+Cl^-}$] is metal-centered, and it is accordingly ascribed to the redox couple $Ru^{3+/2+}$ [53, 54]. The half-wave potential ($E_{1/2}$) of $\mathbf{2^{2+/+}}$ on GC, taken as the average value of the E_p^{ox} and E_p^{red} potentials [55], was determined as $E_{1/2} = -0.818$ V *versus* Ag/AgCl (the half-wave potential with respect to the $Cp_2Fe^{+/0}$ couple is $E_{1/2} = -1.238$ V *versus* $Cp_2Fe^{+/0}$) (Supplementary material, figure S7), and it was found to be independent of v. The anodic and cathodic peak separations, $\Delta E_p = E_p^{ox} - E_p^{red}$, determined on the GC electrode, appears to be higher than the expected theoretical value for one electron-transfer process (0.060 V at 25°C) [56], and tends to increase with increased scan rate. Briefly, in the investigated v range of 0.02–0.12 $V\,s^{-1}$, the determined ΔE_p varies from 0.170 to 0.245 V. It is well known that large ΔE_p values can be attributed either to slow electron-transfer kinetics (quasi-reversible or irreversible process), or to the effect of the uncompensated resistance which is rather significant in solutions of organic solvent media [57]. However, considering that the large amount of uncompensated resistance was already compensated during the measuring process, the obtained large ΔE_p values can be mainly attributed to slow electron kinetics, and thus, the electron transfer process, which occurs on GC, can be interpreted to be quasi-reversible. The ΔE_p values obtained for GC can be used for determination of the heterogeneous electron transfer rate constants (k_s) on this electrode, according to the procedure described in the

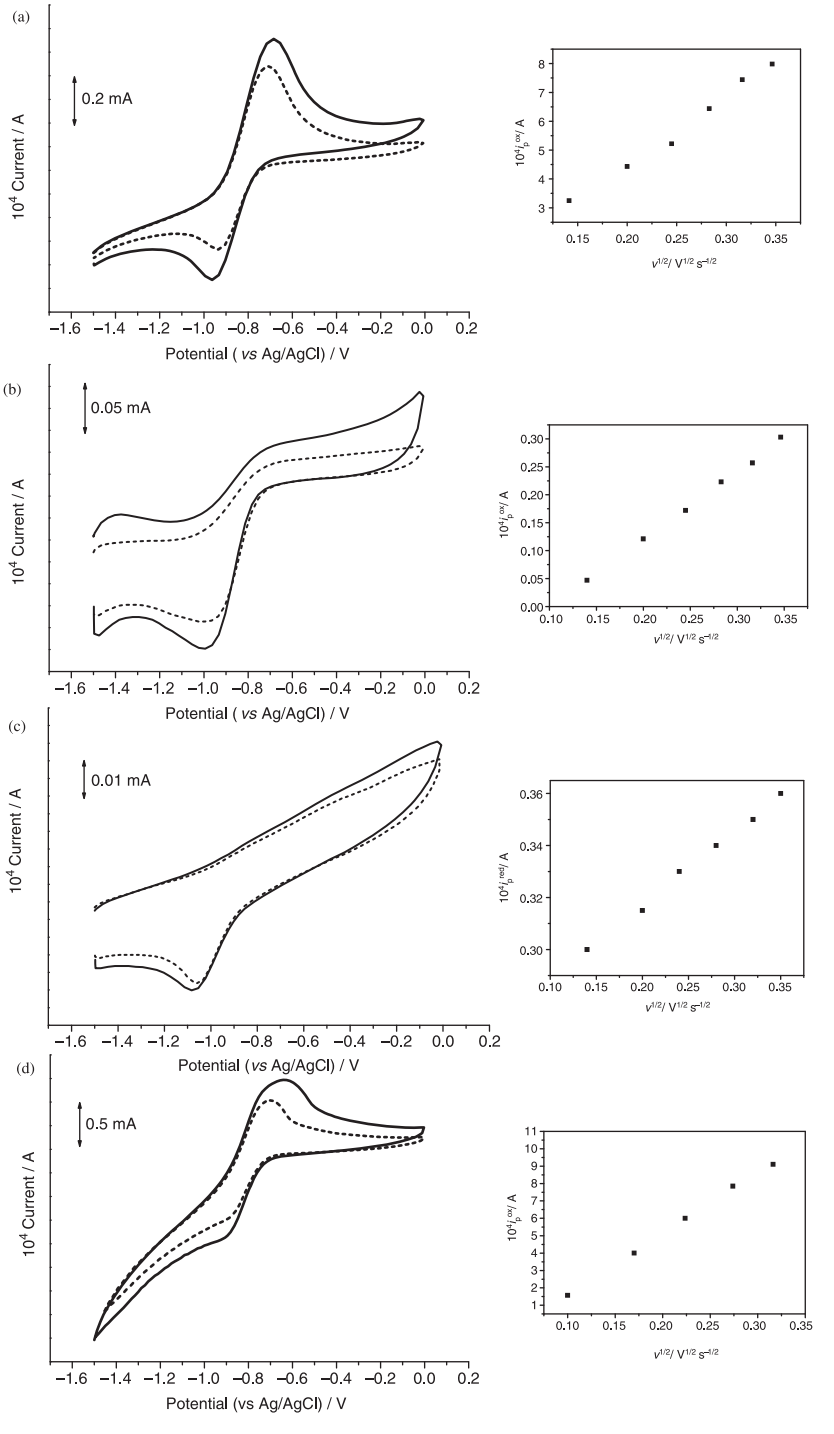

Figure 2. CVs recorded for [$\mathbf{2}^{+}\mathbf{Cl}^{-}$] in ACN on (a) GC, (b) Pt, (c) Au, and (d) MWCNT electrodes at $v = 0.05\,\mathrm{V\,s^{-1}}$ (dotted lines) and $v = 0.10\,\mathrm{V\,s^{-1}}$ (solid lines). The insets exhibit the variation of either the anodic (i_p^{ox}) or the cathodic (i_p^{red}) peak current with the square root of scan rate ($v^{1/2}$).

literature [58]. The determined k_s values on GC, ranging from 1.4×10^{-3} to 0.9×10^{-3} cm s^{-1} (for $0.170 < \Delta E_p < 0.245$), seem to be significantly lower compared to the k_s value obtained for the reversible $Cp_2Fe^{+/0}$ couple on GC in ACN ($k_s = 1.16 \times 10^{-2}$ cm s^{-1}) [59]; but obviously, GC electrode supports faster electron transfer kinetics compared to Pt and Au electrodes. From the CVs shown in figure 2, it can be observed that when GC is replaced with Pt or Au, a noticeable decrease in peak current as well as an increase in the splitting of the peak potentials occur. However, among Pt and Au electrodes, the greatest decrease in the peak current occurs on Au electrode. In detail, the half-wave potential of the $\mathbf{2^{2+/+}}$ redox couple seems to be independent of the working electrode material, and consequently, somehow similar $E_{1/2}$ value for the $\mathbf{2^{2+/+}}$ couple was determined on Pt ($E_{1/2} = -0.814$ V *versus* Ag/AgCl). However, despite both oxidation and reduction peaks being observable in CVs recorded on Pt, rather "disturbed" and not symmetric CVs were obtained, demonstrating that the $\mathbf{2^{2+/+}}$ couple does not illustrate ideal electrochemical behavior on this electrode (figure 2b). Thus, the anodic and cathodic peak current ratios (i_p^{ox}/i_p^{red}) determined on Pt electrode are much less than unity ($i_p^{ox}/i_p^{red} = 0.1$ at $v = 0.04$ V s^{-1}), indicating that the oxidized form of the investigated electro-active compound is probably consumed in a coupled chemical reaction, therefore disturbing the reversibility of the $\mathbf{2^{2+/+}}$ couple. It is, thus, not surprising that significantly greater ΔE_p values were obtained on Pt electrode compared to those determined on GC electrode. Specifically, in the investigated v range 0.02–0.12 V s^{-1}, ΔE_p values in the range 0.286–0.380 V were determined for Pt, leading to k_s values from 0.4×10^{-3} to 0.3×10^{-3} cm s^{-1}. It is clear that among the electrodes tested in this study, the $\mathbf{2^{2+/+}}$ couple demonstrates the greatest deviation from reversibility on Au electrode. On this electrode, the investigated redox couple exhibits the slowest kinetics ($k_s \ll 0.1 \times 10^{-3}$ cm s^{-1}), and thus, the electron transfer process can be characterized as irreversible on Au. As observed in CVs shown in figure 2c, the reduction wave, which corresponds to one electron reduction, $\mathbf{2^{2+}} + e^- \rightarrow \mathbf{2^+}$, and appears at the potential $E_p^{red} = -1.050$ V *versus* Ag/AgCl (at $v = 0.10$ V s^{-1}), was found to be electrochemically irreversible with no anodic reversal current associated with it. In order to test the quality of electrodes used in this study, Cp_2Fe was initially measured under the same experimental conditions. In all cases, Cp_2Fe exhibited reversible oxidation confirming the high quality of the electrodes used. Additional electrochemical experiments performed on a film of MWCNTs demonstrate that this electrode provides fairly fast charge-transfer kinetics for the investigated redox process, which can be compared with that observed on GC (figure 2d). Briefly, from the CVs recorded for [$\mathbf{2^+Cl^-}$] on MWCNT (geometrical area 0.5 cm^2), peak potential separations in the range from 0.182 to 0.248 V (0.02 V s$^{-1} < v < 0.12$ V s^{-1}) were obtained, which result in k_s values from 1.1×10^{-3} to 0.6×10^{-3} cm s^{-1}.

The extracted CV data indicate that within the working electrodes tested both GC and MWCNT electrodes fulfill the conditions to be used for detection of the investigated $\mathbf{2^{2+/+}}$ couple, since the charge transfer process appears to be quasi-reversible on these electrodes. The different electrochemical behaviors observed on Pt and Au electrodes can be attributed to the formation of passive film on electrode surface (chemisorption of electro-active compound on electrode surface), which disturbs the electrochemical reversibility of the redox process. However, further information concerning the sensitivity and thus the quality of the electrodes used can be obtained from EIS experiments.

It would be very interesting to compare the results obtained in this study for $Ru^{3+/2+}$ in [$\mathbf{2^+Cl^-}$] with those reported in the literature for other ruthenium complexes. Srivastava *et al*. [60] investigated the electrochemical behavior of *mer*-[$RuCl_3$(DMSO-S)(DMSO-O)(py)] (where py = pyridine) in DMSO in the scan rate range 0.10–3.0 V s^{-1}. In contrast to the quasi-reversible behavior which displays $Ru^{3+/2+}$ in [$\mathbf{2^+Cl^-}$] in ACN solutions ($0.170\,V < \Delta E_p < 0.245\,V$), the $Ru^{3+/2+}$ couple in *mer*-[$RuCl_3$(DMSO-S)(DMSO-O)(py)] exhibits reversible behavior in DMSO solutions ($0.061\,V < \Delta E_p < 0.096\,V$). Furthermore, the half-wave potential of $E_{1/2} = 0.04$ V *versus* SCE, reported for $Ru^{3+/2+}$ in *mer*-[$RuCl_3$(DMSO-S)(DMSO-O)(py)] in DMSO, can be converted to $E_{1/2} = -0.41$ V *versus* $Cp_2Fe^{+/0}$ [61], which seems to be less cathodic compared to the $E_{1/2}$ obtained in this study for $Ru^{3+/2+}$ in [$\mathbf{2^+Cl^-}$] in ACN ($E_{1/2} = -1.238$ V *versus* $Cp_2Fe^{+/0}$). However, the electrochemical behavior of $Ru^{3+/2+}$ in [$\mathbf{2^+Cl^-}$] seems to be analogous with that of $Ru^{3+/2+}$ in [Ru(DMSO)(bpp)Cl_2] (where bpp = 2,6-*bis*(pyrazol-1-yl)pyridine) and [Ru(DMSO)(bdmpp)Cl_2] (where bdmpp = 2,6-*bis*(3,5-dimethylpyrazol-1-yl)pyridine) complexes in dichloromethane (DCM), reported by Chakrabarty *et al*. [62]. Thus, similar to [$\mathbf{2^+Cl^-}$], in [Ru(DMSO)(bpp)Cl_2] and [Ru(DMSO)(bdmpp)Cl_2] complexes, the redox couple $Ru^{3+/2+}$ exhibits quasi-reversible behavior with peak potential separations of $\Delta E = 0.160$ V and $\Delta E = 0.100$ V, respectively.

3.3. *Electrochemical impedance spectroscopy*

The Nyquist plots recorded for [$\mathbf{2^+Cl^-}$] in ACN on GC, Pt, Au, and MWCNT electrodes are shown in figure 3. In these plots, the complex impedance is presented as a sum of the real (Z_{re}) and imaginary (Z_{im}) components that originate mainly from the resistance and capacitance of the cell, respectively. In general, EIS recorded on GC, Pt, and Au electrodes (figures 3a–3c) include a semicircle portion, observed at higher frequencies, that corresponds to the electron-transfer limited process, followed by a linear part, the Warburg impedance response, appearing at the lower frequency region, which can be attributed to diffusion-limited mass transfer [63]. The respective semicircle diameter, obtained by extrapolation of the semicircle on the Z_{re}-axis, corresponds to the electron transfer resistance (R_{ct}) at the electrode surface, a parameter which is attributed to the electrochemical reaction and provides an estimation not only of the response of the electron transfer but also of the sensitivity of the working electrode [64]. The top of the semicircle corresponds to the frequency (ω): $\omega = 1/(R_{ct}C_{dl})$, where C_{dl} is the double-layer capacity. According to the theory of electrode kinetics [65], development of such semicircles indicates a barrier for the interfacial electron transfer and it can be attributed to an increase of the passivity of the surface of the electrode through formation of a coating. The formation of a surface layer on the electrode is expected to slow down the interfacial charge transfer kinetics, which is reflected by an increase of R_{ct}. The EIS parameters of [$\mathbf{2^+Cl^-}$] on GC, Pt, and Au electrodes were determined by fitting the experimental impedance spectra with the Randles electrical circuit ($R_s + (C_{dl}/R_{ct} + Z_w)$) (Supplementary material, figure S8) [66, 67]. This circuit includes a resistance in series with a parallel combination of a capacitive path and charge- and mass-transfer paths [68]. The elements of the circuit ($R_s + (C_{dl}/R_{ct} + Z_w)$) are explained as follows: R_s is the electrolyte resistance, C_{dl} the double-layer capacitance, R_{ct} the charge-transfer resistance, and Z_W the Warburg impedance,

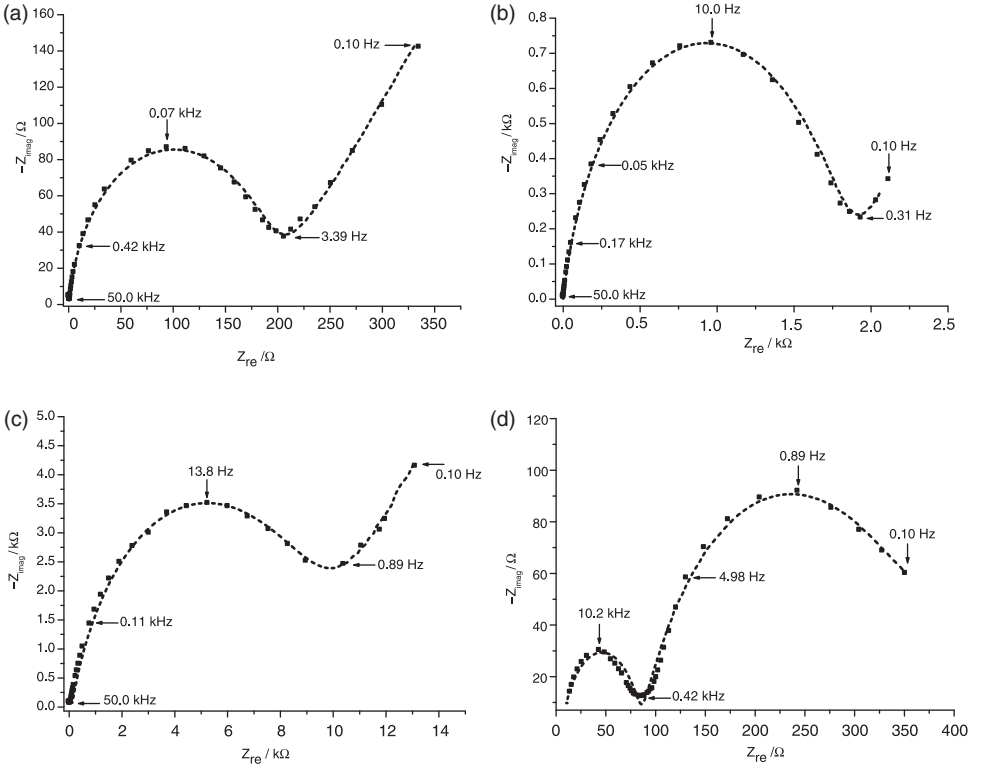

Figure 3. EI spectra recorded for [$\mathbf{2}^{+}\mathbf{Cl}^{-}$] in ACN on (a) GC, (b) Pt, (c) Au, and (d) MWCNT electrodes in the frequency range from 0.1 Hz to 50 kHz. The EI spectra were recorded at the formal potential of the $\mathbf{2}^{2+/+}$ redox couple ($E_{1/2} = -0.818$ V *vs.* Ag/AgCl). The electrolyte resistance was subtracted from Z_{re}-axis. The electrical equivalent circuits used for fitting the recorded EI spectra are reported in "Supplementary material" (figures S8 and S9).

which is connected with the parameter σ through the relation $Z_W = \sigma/(i\omega)^{1/2}$, where ω represents the frequency [69]. The Warburg parameter σ is strongly dependent on the diffusion ability of the electro-active species, namely σ is inversely analogous to the diffusion coefficients of the oxidized and reduced species. The solution resistances were found to be about $R_s \approx 35 \pm 5\,\Omega$ in all experiments. The R_{ct} values indicate that the resistance for the electron transfer process increases in the following order: GC ($R_{ct} = 0.19\,k\Omega$) < Pt ($R_{ct} = 1.82\,k\Omega$) < Au ($R_{ct} = 10.08\,k\Omega$). Furthermore, the Warburg σ parameters reveal that the diffusion ability of the reactants is enhanced on GC electrode, while their ability for diffusion is rather small on Au electrode: GC ($\sigma = 0.16\,k\Omega\,s^{-1/2}$) < Pt ($\sigma = 0.29\,k\Omega\,s^{-1/2}$) < Au ($\sigma = 3.86\,k\Omega\,s^{-1/2}$). The decrease of the Warburg σ coefficient is associated with increase of diffusion of the electro-active species [70]. The obtained impedance results are in accordance with those extracted from the CV studies. Consequently, on GC electrode, which is characterized by the smallest R_{ct} and the lowest Warburg parameter σ, fast electron-transfer kinetics (either reversible or quasi-reversible process) would be expected, while on Au electrode, with the maximal values of R_{ct} and σ, an irreversible electron transfer would occur. The large R_{ct} values obtained for Pt and Au electrodes verify the formation of coating on their

surface leading, therefore, to an increase of their passivity. It is also interesting that the C_{dl} values were found to increase in the following order: Au ($C_{dl} = 0.471\,\mu F$) < Pt ($C_{dl} = 4.108\,\mu F$) < GC ($C_{dl} = 9.766\,\mu F$), indicating that the GC electrode is the "best" double-layer capacitor. Considering that the ability of a capacitor to store electric charge is strongly dependent on its available area, the findings demonstrate that the GC electrode has greater active surface area compared to that of Pt and Au electrodes. From the Warburg coefficients determined, the active surface areas of the electrodes GC (0.124 cm^2), Pt (0.068 cm^2), and Au (0.005 cm^2) were estimated. The findings verify once more that the Au and Pt electrodes exhibit enhanced passivity.

The EI spectrum obtained on MWCNT differs from those recorded on GC, Pt, and Au electrodes. Thus, the main characteristics of the Nyquist plot are two semicircles over the entire frequency range (the low frequency linear-mass-transfer portion is not observable; figure 3d). The presence of two semicircles in the impedance spectrum indicates that the system MWCNT/[$\mathbf{2^+Cl^-}$]/TBAPF$_6$ is non-ideal and this can be explained by incorporating additional circuit elements in the Randles circuit. Consequently, for fitting the EIS data obtained on MWCNT, the equivalent electrical circuit ($R_s + (C_f/R_f + (C_{dl}/R_{ct} + Z_w))$) was applied (Supplementary material, figure S9). The occurrence of the high-frequency semicircle in the EI spectrum is explained by an additional resistance R_f (0.08 kΩ) and capacitance C_f (0.37 μF), which can be associated with the surface of the MWCNT film [71]. The charge transfer resistance of [$\mathbf{2^+Cl^-}$] on MWCNT film ($R_{ct} = 0.28\,k\Omega$) is slightly higher than that obtained on GC ($R_{ct} = 0.19\,k\Omega$) and significantly slower to those estimated on either Pt ($R_{ct} = 1.82\,k\Omega$) or Au ($R_{ct} = 10.08\,k\Omega$) electrodes. The impedance results are in very good agreement with the recorded CVs. Thus, the charge-transfer resistance of [$\mathbf{2^+Cl^-}$] on various electrodes decreases with the order Au > Pt > MWCNT > GC, implying that both GC and MWCNT provide an insignificant barrier toward charge transfer and consequently faster electrode kinetics, while Pt, and much more Au, prevent the charge-transfer process.

4. Conclusions

The aim of this study was the electrochemical investigation of **1** in ACN on various working electrodes. For this purpose, conductivity, CV, EIS, and ESI–MS were applied. For the electrochemical experiments, conventional electrodes such as GC, Pt, and Au were used. Furthermore, a film of MWCNT was also used as a working electrode. Qualitative examination of the **1**/ACN system by means of conductance and ESI–MS demonstrates that upon dissolution of **1** in ACN replacement of one chloro- and one PPh_3 ligand by ACN occurs, resulting in formation of the 1 : 1 type electrolyte [$\mathbf{2^+Cl^-}$]. The CV findings suggest that the redox couple $\mathbf{2^{2+/+}}$ is quasi-reversible on either GC or MWCNT electrodes and irreversible on Au electrode. The rate of the electron transfer diminishes in the following order: GC ($k_s \approx 1.5 \times 10^{-3}$) > MWCNT ($k_s \approx 0.9 \times 10^{-3}\,cm\,s^{-1}$) > Pt($k_s \approx 0.4 \times 10^{-3}\,cm\,s^{-1}$) > Au($k_s \ll 0.1 \times 10^{-3}\,cm\,s^{-1}$). The impedance data obtained for GC, Pt, and Au can be described by means of Randles electrical circuit, while for analysis of the impedance response of MWCNT an additional resistance and capacitance, associated with the film surface, must be considered. The findings reveal that the rate of electron transfer on either GC or

MWCNT is enhanced due to the small charge-transfer resistance and thus to the insignificant barrier for interfacial electron transfer, which is provided from these particular electrodes.

Acknowledgments

The authors thank Mrs S. Heusing and Mrs D. Schneider (TU Ilmenau). A.I. Philippopoulos thanks the special research account of the National and Kaposistrian University of Athens for the financial support (Kapodistrias program number: 70/4/9277). The mass spectrometric work in Prague was supported by the Academy of Sciences of the Czech Republic (Z40550506), the European Research Council (AdG HORIZOMS), and the Grant Agency of the Czech Republic (203/08/1487).

References

[1] R.E. Clarke, P.C. Ford. *Inorg. Chem.*, **9**, 227 (1970).
[2] H.S. Lim, D.J. Barclay, F.C. Anson. *Inorg. Chem.*, **11**, 1460 (1972).
[3] S.A. Adeyemi, J.N. Braddock, G.M. Brown, J.A. Ferguson, F.J. Miller, T.J. Meyer. *J. Am. Chem. Soc.*, **94**, 300 (1972).
[4] S.A. Adeyemi, E.C. Johnson, F.J. Miller, T.J. Meyer. *Inorg. Chem.*, **12**, 2371 (1973).
[5] A.W. Zanella, P.C. Ford. *Inorg. Chem.*, **14**, 42 (1975).
[6] R.W. Callahan, G.M. Brown, T.J. Meyer. *Inorg. Chem.*, **14**, 1443 (1975).
[7] S.E. Diamond, G.M. Tom, H. Taube. *J. Am. Chem. Soc.*, **97**, 2661 (1975).
[8] K. Rieder, U. Hauser, H. Siegenthaler, E. Schmidt, A. Ludi. *Inorg. Chem.*, **14**, 1902 (1975).
[9] T. Matsubara, P.C. Ford. *Inorg. Chem.*, **15**, 1107 (1976).
[10] D. Mishra, S. Naskar, A.J. Blake, S.K. Chattopadhyay. *Inorg. Chim. Acta*, **360**, 2291 (2007).
[11] Md.K. Nazeeruddin, C. Klein, P. Liska, M. Grätzel. *Coord. Chem. Rev.*, **249**, 1460 (2005).
[12] Z.-S. Wang, H. Kawauchi, T. Kashima, H. Arakawa. *Coord. Chem. Rev.*, **248**, 1381 (2004).
[13] J. Faiz, A.I. Philippopoulos, A.G. Kontos, P. Falaras, Z. Pikramenou. *Adv. Funct. Mater.*, **17**, 54 (2007).
[14] A.I. Philippopoulos, A. Terzis, C.P. Raptopoulou, V.J. Catalano, P. Falaras. *Eur. J. Inorg. Chem.*, 5633 (2007).
[15] A. Juris, V. Balzani, F. Barigelletti, S. Campagna, P. Belser, A. Zelewsky. *Coord. Chem. Rev.*, **84**, 85 (1988).
[16] V. Balzani, A. Juris, M. Venturi, S. Campagna, S. Serroni. *Chem. Rev.*, **96**, 759 (1996) (and references therein).
[17] Z. Zhou, G.H. Sarova, S. Zhang, Z. Ou, F.T. Tat, K.M. Kadish, L. Echegoyen, D.M. Guldi, D.I. Schuster, S.R. Wilson. *Chem. Eur. J.*, **12**, 4241 (2006).
[18] M. Auzias, B. Therrien, G. Süss-Fink, P. Stepnicka, W.H. Ang, P.J. Dyson. *Inorg. Chem.*, **47**, 578 (2008).
[19] A.M. Joshi, I.S. Thorburn, S.J. Rettig, B.R. James. *Inorg. Chim. Acta*, **198–200**, 283 (1992).
[20] D.E. Fogg, B.R. James, M. Kilner. *Inorg. Chim. Acta*, **222**, 85 (1994).
[21] S.E. Clapham, A. Hadyovic, R.H. Morris. *Coord. Chem. Rev.*, **248**, 2201 (2004).
[22] R. Noyori, T. Ohkuma. *Angew. Chem. Int. Ed.*, **40**, 40 (2001).
[23] A. Demonceau, F. Simal, A.F. Noels, C. Viñas, R. Nuñez, F. Teixidor. *Tetrahedron Lett.*, **38**, 4079 (1997).
[24] E.M. Sussuchi, A.A. de Lima, W.F. De Giovani. *Polyhedron*, **25**, 1457 (2006).
[25] F. Hartl, T. Mahabiersing, P. Le Floch, F. Mathey, L. Ricard, P. Rosa, S. Záliš. *Inorg. Chem.*, **42**, 4442 (2003).
[26] S. Kasselouri, A. Garoufis, A. Katehanakis, G. Kalkanis, S.P. Perlepes, N. Hadjiliadis. *Inorg. Chim. Acta*, **207**, 255 (1993).
[27] P.S. Hallman, T.A. Stephenson, G. Wilkinson. *Inorg. Synth.*, **12**, 237 (1970).
[28] N.G. Tsierkezos, A.I. Philippopoulos. *Inorg. Chim. Acta*, **362**, 3079 (2009).
[29] J.E. Lind Jr, J.J. Zwolenik, R.M. Fuoss. *J. Am. Chem. Soc.*, **81**, 1557 (1959).

[30] N.G. Tsierkezos, I.E. Molinou. *Z. Phys. Chem.*, **216**, 961 (2002).
[31] N.G. Tsierkezos. *Z. Phys. Chem.*, **222**, 63 (2008).
[32] C.N.R. Rao, R. Sen. *Chem. Commun.*, 1525 (1998).
[33] B.C. Satishkumar, A. Govindaraj, C.N.R. Rao. *Chem. Phys. Lett.*, **307**, 158 (1999).
[34] N.G. Tsierkezos, U. Ritter. *J. Solid State Electrochem.*, **14**, 1101 (2010).
[35] J. Roithová, D. Schröder. *Phys. Chem. Chem. Phys.*, **9**, 731 (2007).
[36] J. Roithová, D. Schröder, J. Mišek, I.G. Stará, I. Starý. *J. Mass Spectrom.*, **42**, 1233 (2007).
[37] N.B. Cech, C.G. Enke. *Mass Spectrom. Rev.*, **20**, 362 (2001).
[38] D. Schröder, T. Weiske, H. Schwarz. *Int. J. Mass Spectrom.*, **219**, 729 (2002).
[39] B. Das, N. Saha. *J. Chem. Eng. Data*, **45**, 2 (2000).
[40] T.J. Huttemann, B.M. Foxman, C.R. Sperati, J.G. Verkade. *Inorg. Chem.*, **4**, 950 (1965).
[41] M.W. Duckworth, G.W.A. Fowles, R.A. Hoodless. *J. Chem. Soc.*, 5665 (1963).
[42] J.V. Quagliano, J.T. Summers, S. Kida, L.M. Vallarino. *Inorg. Chem.*, **3**, 1557 (1964).
[43] R.A. Walton. *Q. Rev. Chem. Soc.*, **19**, 126 (1965).
[44] W.J. Geary. *Coord. Chem. Rev.*, **7**, 81 (1971).
[45] L.F. Silva, N.P. Lopes. *Tetrahedron Lett.*, **46**, 6023 (2005).
[46] V.B. Di Marco, G.G. Bombi. *Mass Spectrom. Rev.*, **25**, 347 (2006).
[47] N.G. Tsierkezos, J. Roithová, D. Schröder, I.E. Molinou, H. Schwarz. *J. Phys. Chem. B*, **112**, 4365 (2008).
[48] N.G. Tsierkezos, J. Roithová, D. Schröder, M. Ončák, P. Slaviček. *Inorg. Chem.*, **48**, 6287 (2009).
[49] A.V. Sechkarev, Y.A. Fadeev, I.D. Reva. *J. Appl. Spectrosc.*, **66**, 708 (1999).
[50] W.H. Lee, R.J. Wheaton. *J. Chem. Soc., Faraday Trans.*, **74**, 1456 (1978).
[51] W.H. Lee, R.J. Wheaton. *J. Chem. Soc., Faraday Trans.*, **75**, 1128 (1979).
[52] N.G. Tsierkezos, A.I. Philippopoulos. *Fluid Phase Equilib.*, **277**, 20 (2009).
[53] S. Priyarega, R. Prabhakaran, K.R. Aranganayagam, R. Karvembu, K. Natarajan. *Appl. Organomet. Chem.*, **21**, 788 (2007).
[54] T.D. Thangadurai, K. Natarajan. *Transition Met. Chem.*, **25**, 347 (2000).
[55] M.T. Carter, M. Rodriguez, A.J. Bard. *J. Am. Chem. Soc.*, **111**, 8901 (1989).
[56] J. Qiu, K. Matyjaszewski, L. Thouin, C. Amatore. *Macromol. Chem. Phys.*, **201**, 1625 (2000).
[57] A.M. Bond, K.B. Oldham, G.A. Snook. *Anal. Chem.*, **72**, 3492 (2000).
[58] R.S. Nicholson. *Anal. Chem.*, **37**, 1351 (1965).
[59] N.G. Tsierkezos, U. Ritter. *J. Appl. Electrochem.*, **40**, 409 (2010).
[60] R.S. Srivastava, F.R. Fronczek, R.S. Perkins. *J. Coord. Chem.*, **62**, 3745 (2009).
[61] N.G. Connelly, W.E. Geiger. *Chem. Rev.*, **96**, 877 (1996).
[62] S. Chakrabarty, P. Sarkhel, R.K. Poddar. *J. Coord. Chem.*, **63**, 1563 (2010).
[63] A. Bardea, F. Patolsky, A. Dagan, I. Willner. *Chem. Commun.*, 21 (1999).
[64] M.J. Esplandiu, M. Pacios, E. Bellido, M. Del Valle. *Z. Phys. Chem.*, **221**, 1161 (2007).
[65] E. Gileadi. *Electrode Kinetics for Chemists, Chemical Engineers, and Materials Scientists*, VCH Publishers, Weinheim, Germany (1993).
[66] J.E.B. Randles. *Trans. Faraday Soc.*, **44**, 327 (1948).
[67] K.J. Vetter. *Electrochemical Kinetics*, Academic Press, New York (1967).
[68] S. Omeiri, B. Bellal, A. Bouguelia, Y. Bessekhouad, M. Trari. *J. Solid State Electrochem.*, **13**, 1395 (2009).
[69] F. Koeleli, T. Roepke, C.H. Hamann. *Electrochim. Acta*, **48**, 1595 (2003).
[70] Y. Zhang, M. Urquidi-Macdonald. *J. Power Sources*, **129**, 312 (2004).
[71] N. Sharma, M. Deepa, S.A. Agnihotry. *Solid State Ionics*, **152–153**, 873 (2002).